SLAC-PUB-10883
Revised - February 2008

An acoustic sensor system for localizing RF breakdown in warm copper accelerating structures

F. Le Pimpec*, J. Frisch, K. Jobe, D. McCormick, J. Nelson, M. Ross, T. Smith

SLAC, 2575 Sand Hill Road, Menlo Park, CA 94025, USA

Abstract

X-band accelerator structures meeting the Next Linear Collider (NLC) design requirements have been found to suffer damage due to Radio Frequency (RF) breakdown when processed to high gradients [F. Le Pimpec, et al., in: LINAC 2002, Korea, SLAC-PUB-9526, 2002 [1]]. Improved understanding of these breakdown events is desirable for the development of structure designs, fabrication procedures, and processing techniques that minimize structure damage. Acoustic sensors attached to an accelerator structure can detect both normal and breakdown RF pulses [M. Gangeluk, et al., Acoustic monitoring system of RF breakdowns inside the electrodynamics structure at Kurchatov SR source accelerator, in: EPAC, P.1986, 1994 [2]]. Using an array of acoustic sensors, we have been able to pinpoint both the cell and azimuth location of individual breakdown events. This permits studies of breakdown in time and in space, so that underlying causes can be determined. This technique provided a significant understanding of breakdown in the structure input coupler.

Keywords: 43.60.+d; 68.35.Iv; 52.80.Pi; 29.17.+w

Keywords: Acoustic sensor; Acoustic wave; RF breakdown; Copper structure; RF structure; X-band; Phonon

1. Introduction

In the framework of the International Linear Collider (ILC), two accelerator designs were in competition, one based on an RF warm copper structure, and one based on superconductive RF technology. The ILC is going to be a "cold" machine. Results and techniques presented in this paper were developed for the abandoned warm design.

As part of the (now terminated) R&D effort for the Next Linear Collider (NLC), the achievement of high gradients (70 MV/m) with a breakdown rate of 1 per 10 h must be demonstrated [3,4]. In the Next Linear Collider Test Accelerator (NLCTA), at SLAC (Stanford Linear Accelerator Center), RF travelling wave, but also standing wave, copper structures designed to meet the needs of the NLC [5] were tested.

To reach an NLC accelerating field of 70 MV/m with a 400 ns pulse length, the power input into these structures is in the megawatt range. Depending on the design and type of the structure, this power can vary from 73 MW for a 60 cm long travelling wave structure with a 3% group velocity (H60VG3) to 150 MW for some of the first structures of 180 cm length. A part of this RF power is lost in the copper and transformed into heat. The lost power is up to $\frac{2}{3}$ of the input power for a structure kept at 45 °C. The thermal expansion of the copper, as the structures fill with RF power, causes sound, which occurs on every machine pulse. Using extremely sensitive piezoelectric microphones, or acoustic sensors, it is possible to "listen" to the accelerator structure as it is running [2], cf Fig. 1.

High gradient is obtained by exposing the structure to High Power Pulsed (HPP) RF. This technique is called RF processing. During processing the structures occasionally respond by arcing, or breakdown. A breakdown is characterized by a shut off of the transmitted power and

*Corresponding author.
E-mail address: frederic.le.pimpec@psi.ch (F. Le Pimpec).

Submitted to Nuclear Instrumentation and Methods (NIM) A
Work supported by US Department of Energy contract DE-AC02-76SF00515

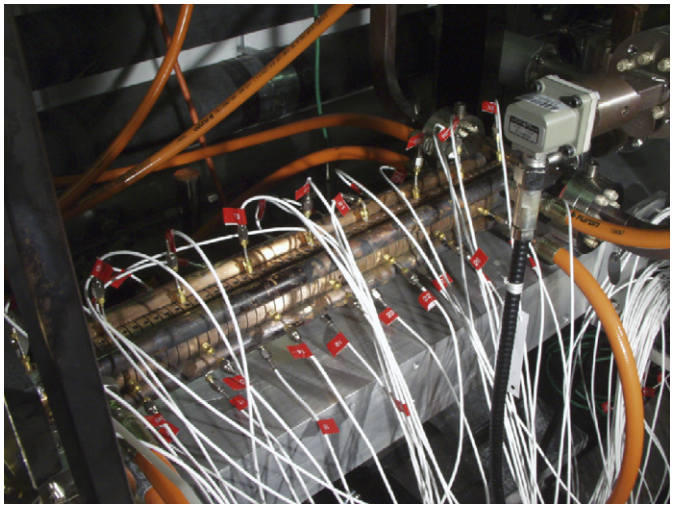

Fig. 1. T53VG3RA (53 cm long travelling wave structure of 3% group velocity) structure covered with acoustic sensors.

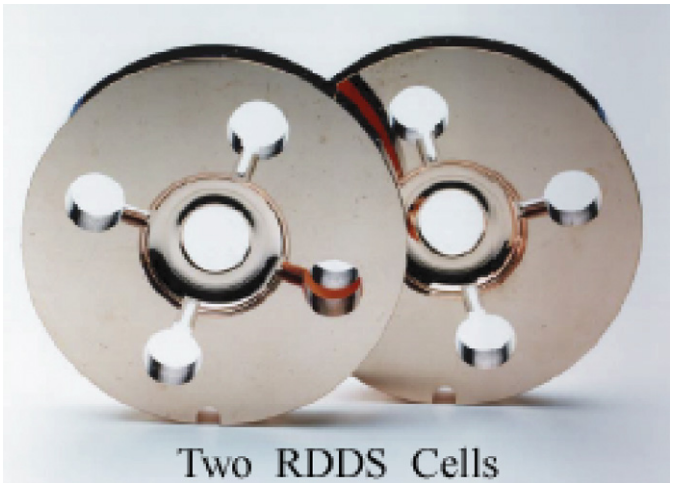

Fig. 2. Rounded damped and detuned NLC type accelerator cell structure.

up to 80% of the incident power is absorbed in the arc [6]. This extra energy is deposited in the copper, and a part of it is converted into extra phonons (heat and acoustic) that can be picked up by our acoustic sensors. With this technique, crude localization of a breakdown is straightforward, and complementary to the standard RF analysis with directional RF couplers. As the RF analysis of a breakdown signal can provide its localization on line, it seems that using acoustic sensors to locate breakdown is superfluous. We will, however, show that acoustic sensors are not only complementary to RF analysis, but also they impacted on the attainment of high gradient.

2. Breakdowns, copper and acoustic limitation

In order to achieve an accelerating voltage equal to the design parameter needed for the NLC, the RF accelerating structures are subjected, before HPP, to a series of chemical and heat processes, which can be called pre-processing. This pre-processing is intended to "clean" the surface from contaminants which can trigger RF breakdown. The use of acoustic sensors in the domain of accelerator operations is rather new and it seems reasonable to summarize briefly the implication of the pre-processing on the acoustic propagation.

After the chemical etching of the cells, the structures are either bonded in a hydrogen atmosphere (SLAC treatment) or brazed under argon atmosphere (FNAL treatment). Any gas dissolved in the copper is outgassed by a vacuum firing. The temperature involved in the thermal treatment varies from 600 to 1000 °C. At these temperatures, grains are growing and recrystallization occurs. The speed of sound in copper is dependant on the form of, and the treatment received by, the copper [7]. Hence, the grain size of the material is a limiting factor, due to the diffraction of the waves, for the choice of an acoustic sensor. The typical grain size of the copper, in the cells, is a millimeter. For pressure waves of 4760 m/s [7] the diffraction limit is achieved at 4.7 MHz. Local plasticity due to the intake of hydrogen, can also affect the propagation of the acoustic waves inside the copper [8]. It is not clear if the vacuum firing, outgassing the hydrogen, will stress relax the crystalline structure of the copper.

The choice of adequate sensors for localization is then dependant, not only on the pickup properties of the sensor but also on the frequencies of the acoustic waves to be analyzed. Hence, the resolution which can be achieved by an array of these sensors depends on the diffraction limits, the attenuation of the different types of waves, pressure waves, shear waves and surface waves (Rayleigh waves) [9,10] as well as any anisotropy of the medium [11]. Finally, the complex geometry of the cells forming the structure is also an extra challenge to the resolution, Fig. 2.

3. Acoustic sensors and data acquisition system

3.1. Acoustic sensors

Since the first report on this technique [12] several commercial sensors of the kind used to monitor microscopic cracks in bridges or airplane frames, as well as SLAC-made sensors, Fig. 3, have been tested and used [13].

Most of the results presented in this paper were obtained using the sensor shown in Fig. 3. The sensor is made of a piezoelectric ceramic, soldered onto a copper piece. A conductor is then soldered onto the back of the ceramic and connected to an SMA connector. The ceramic is embedded in a Room Temperature Vulcanizing (RTV) silicon which act as a damping material. The power response in dB versus frequency of the SLAC sensor is given in Fig. 4 when it is driven by a commercial microdot 100 sensor, Fig. 5.

Sensors are glued on the structure by the use of fast drying Loctite. The use of a hardener, sprayed on the structure when the sensors are pressed onto it, helps to

Fig. 3. SLAC type acoustic sensor 200 kHz–1.5 MHz.

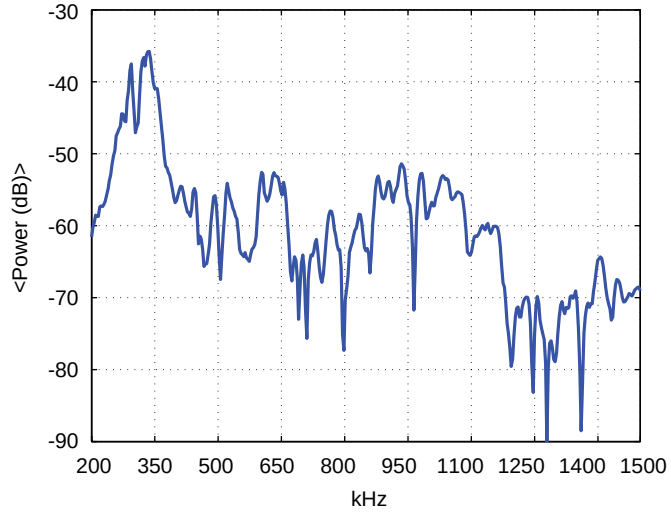

Fig. 4. Homemade SLAC sensor frequency response, when driven by a Microdot 100 Sensor. The signal is analyzed via a network analyzer. Sensors are held together with a pinch clamp and vacuum grease in between.

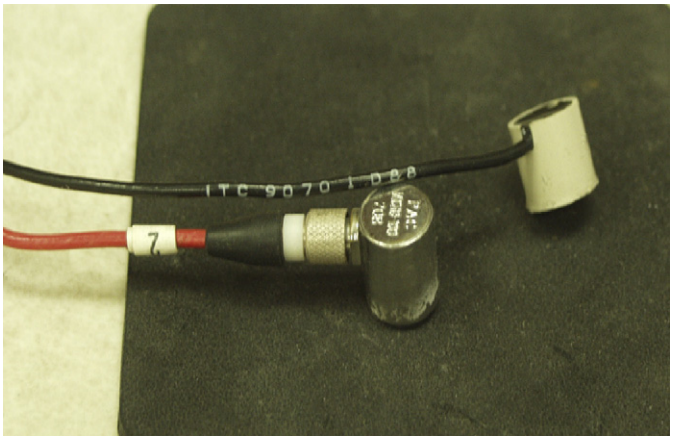

Fig. 5. Microdot 100 and ITC 9070 (white sensor with black cable).

ensure good contact. With this technique, we also obtain a better reproducibility of the contact between the sensor and the copper structure. Loose or shaky contact can lead to a drastic reduction of the recorded signal. Due to our requirements, we are now using commercial sensors ITC-9070 from *International Transducer Corporation*, Fig. 5.

3.2. Electronics and DAQ system

An array of up to 64 sensors (limited by DAQ channels) is attached to the accelerator structure to locate breakdowns. Radiation in the accelerator tunnel prevents the use of local electronics and the sensors are transformer coupled to drive differential pair cables. A differential receiver and amplifier are used in the control area, followed by a digitizer (Fig. 6).

3.3. Analog electronics

The acoustic sensors act approximately as current sources in parallel with about 1000 pf of capacitance. For 300 kHz signals this corresponds to 500 Ω impedance. The sensor is connected to a 400 : 100 Ω transformer driving 100 Ω twisted pair (Cat-5 Telecom) cable, with impedance matching to 50 Ω at the receiver. The Cat-5 is useful because it does not pick up noise and has a low cost. A variable gain amplifier is used to match the signal level into the digitizer input [13].

3.4. Digital electronics and software

The digitizers used are Joerger VTR812-10, eight channel, 12 bit, 10 Ms/s VME modules with input range ±2 V and 50 Ω input. Eight modules were used for a total of 64 channels. The modules are operated in circular buffer mode to record the last three events, with 1024 points per event, as represented in Fig. 7. The n pulse being the RF pulse when the structure breaks down, the $(n-1)$ and $(n-2)$ pulses should be normal pulses, or background noise of the RF power. Fig. 7 is a 2D representation of a 3D plot. The abscisse represents the three sets of pulses of 1024 points each. The right ordinate is the number of sensors, each line being one sensor. The data displays the response of 13 sensors with sensor 1 being a broken, flat line. The left ordinate is the intensity recorded for each sensor in mV.

The control system is based on EPICS® and operates both the RF level control for processing and the acoustic data acquisition. When the processing system detects a RF breakdown, the next RF pulse is disabled and the data from all of the digitizers for the last three pulses is recorded. Data is processed offline using Matlab®. Typically the RMS of the first 200 points (20 μs or 10 mm at copper P-wave velocity 4760 m/s) is used to determine the breakdown location.

4. Sensor calibration

Absolute calibration of acoustic sensors is not trivial in the frequency range of interest, some of the problem arising due to the imperfect nature of the transfer block used in between the sensors. Also, the repeatability between measurements after dismounting the system and remounting is poorer than without remounting [14]. A way we

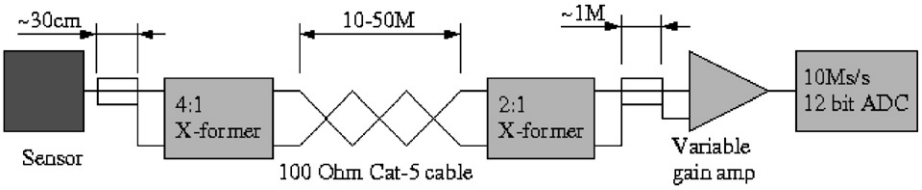

Fig. 6. Electronics block diagram.

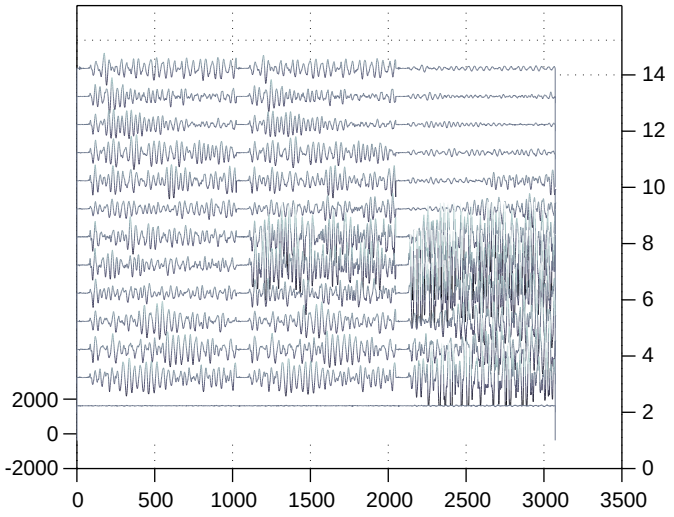

Fig. 7. Sequence of three pulses in T53VG3F, 53 cm long travelling wave structure with 3% group velocity.

found to calibrate our sensor is to use the RF power dissipated in our copper structure. The RF losses inside the structure will induce a mass movement of the copper due to thermal expansion. The temperature rise of the overall accelerating structure, cooled with water, is slow and only of a few °C. It is then reasonable to consider the thermal properties of the copper constant during the RF pulse. We expect the response of the sensors to be linear with the power loss in the structure [12]. Results with RF pulses at 100, 170, 240 and 400 ns have been recorded for three structures and one set of results is displayed in Fig. 8. The measurements in Fig. 9, were carried out by using an artificial trigger, in order to avoid data corruption by RF breakdown. The RF structure was monitored by nine sensors and the data recorded over the full memory of the module.

The RMS response in mV of the sensors versus the RF power flowing inside the structure, for example as shown in Fig. 8, confirms the results obtained in Ref. [12]. Results obtained for the sensors at other RF pulse lengths are similar. Data can be fitted with a linear equation showing the dependencies of the effect of thermal heating by the RF vs the acoustic response of the sensor. We can see in Fig. 8 the very good agreement between the data and the linear fit. Fig. 10 displays the standard deviation [15] of the difference between the data set and its fit, for 64 sensors. The results show that the difference between the data and the fit is around 2 mV (cross and circle). However, some sensors have a much larger deviation (circles). Fig. 11 displays the difference at a given power between the data and their fit for 64 sensors (the error bar is the response in mV of the sensor). The data Set #2 at RF power of 58 MW has a variation of the response which is much larger that at any other RF power: 20 mV compared to 2 mV. Thus the real accuracy of the fit to the data in Fig. 8 is given by the cross set in Fig. 10, after data set #2 has been withdrawn from the standard deviation calculation.

In some cases, the expected trend was not obtained for some sensors. In those cases a bad contact between the sensor and the structure, or a deficient sensor, was responsible. As an example, Fig. 9 displays the typical response of acoustic sensors when normal pulsed RF is fed into the structure. A defective sensor, third signal line in Fig. 9, shows a flat line.

The purpose of doing a HPP processing [16], or RF processing, is to reach a given electric field value without arcing in the structure. Since data reduction is performed offline, sensor calibration can be performed after the end of the processing of the structure, or before switching from one RF pulse length to another. A possible method to account for energy deposition in the structure when an arc occurs, could be to use the acoustic calibration curve associated with the RF power lost in the structure without breakdown, for example as in Fig. 8.

It has to be noted that simple calculation will show that the radiation pressure of the RF wave can be neglected in comparison to the following sound wave created by the rise of temperature in the structure due to RF losses.

As an absolute calibration is not yet in reach, we might use a relative calibration, Fig. 12. A set of data is recorded at a given pulse length and a ratio of the output of the voltage versus one of the sensors is calculated. The data are recorded in three sequences of 1024 points corresponding to three consecutive RF pulses, Fig. 7. We have chosen to calculate the sensitivity based on the first 200 points or 20 μs of the signal.

As we can see in pulse $(n-1)$, Fig. 7, breakdown can occur without shutting off the klystron. Normally, when the accelerator software "detects" a breakdown, the power in the klystron is shut down for the next minute, and the acoustic data are recorded. Consequently, it is better to use the $(n-2)$ pulse to calculate the relative sensitivity after each breakdown. However, in very rare cases, we have seen breakdown in pulse $(n-2)$; but with an occurrence of less than 1%. Also, during operation sensors can fall off the

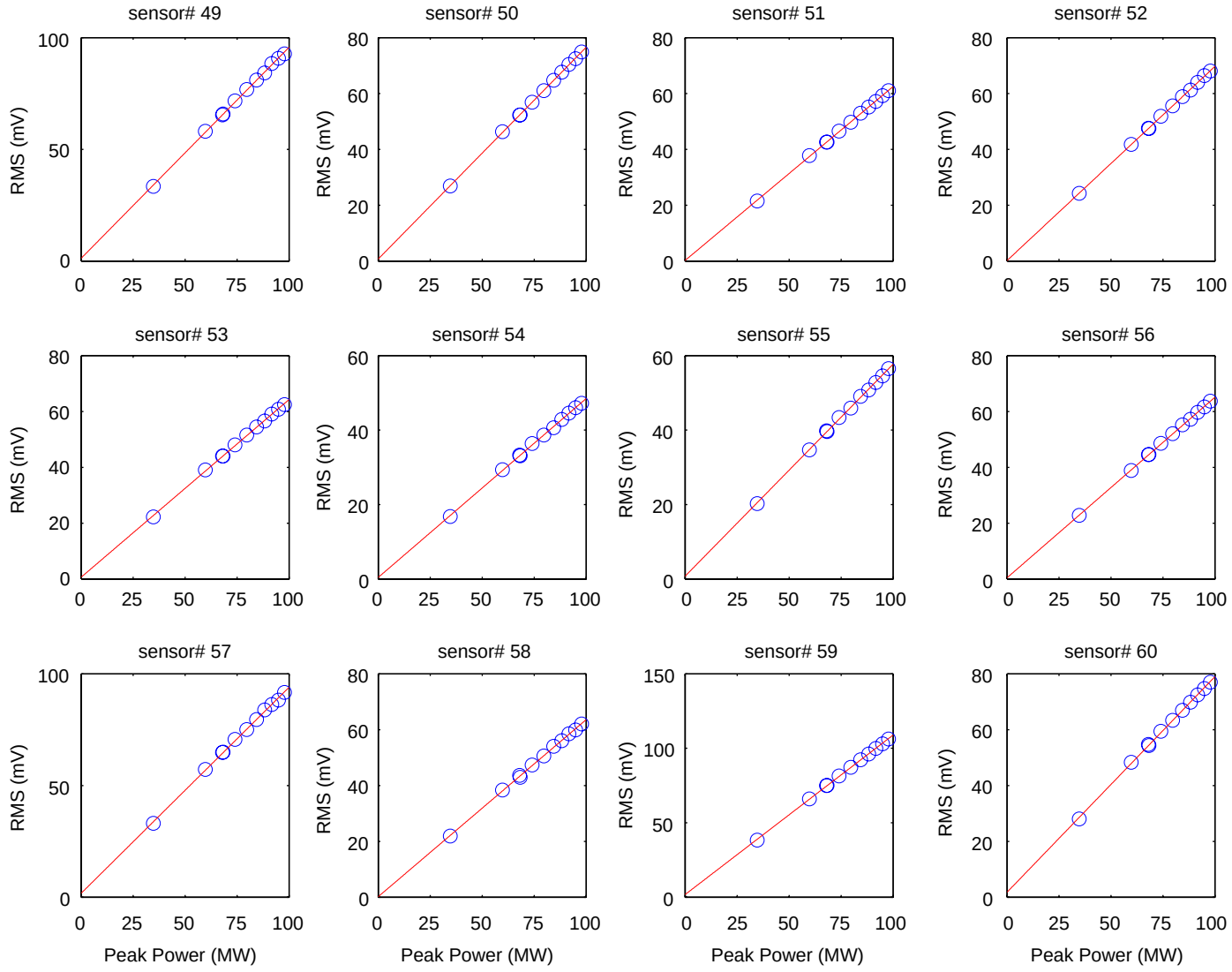

Fig. 8. ITC-9070 sensor calibration with a 400 ns RF pulse length with various RF powers in H60VG3R structure. RMS of the first 20 μs of the signal. The straight line is a linear fit.

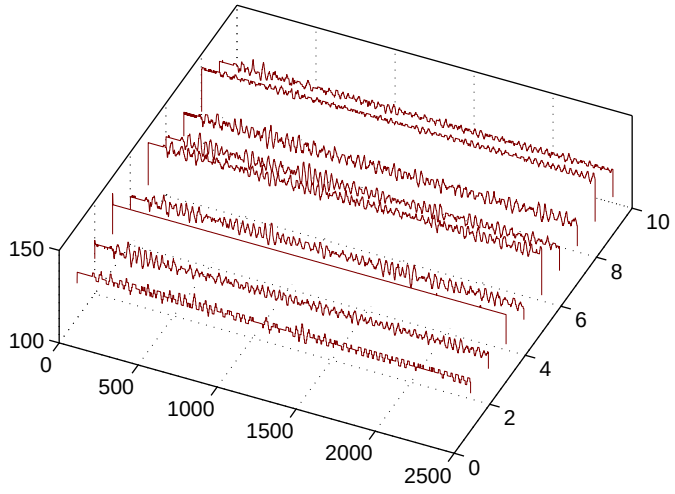

Fig. 9. Acoustic sensors' response (nine sensors) to a 100 ns RF pulse length and 150 MW RF power in T53VG3R structure.

structure, or break, as the first sensor in Fig. 7. Since data are not looked at on a day to day basis but analyzed automatically, we might not be able to fix the problem in a reasonable time. Also as the processing evolves, the sensors are exposed to higher X-rays doses and we should consider the possibility that the initial relative calibration can shift with time. Whatever the mechanisms are, which induce a shift in the response of the sensor, we will refer to them by the general term of "ageing" of the sensors.

For most of our analysis some general relative sensitivity files were used. These files were updated from time to time to take into account the ageing of the sensors. We found out that results of coarse localization of breakdown, whether or not we used those files, were very similar. Precise localization, for instance localizing where on a cell the breakdown has deposited the most energy, required frequent updating of these files.

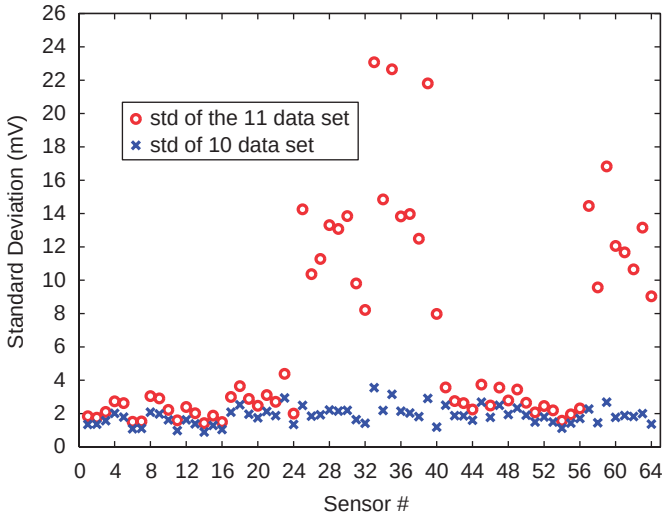

Fig. 10. Standard deviation of the difference between the data set of a given sensor and its associated fit.

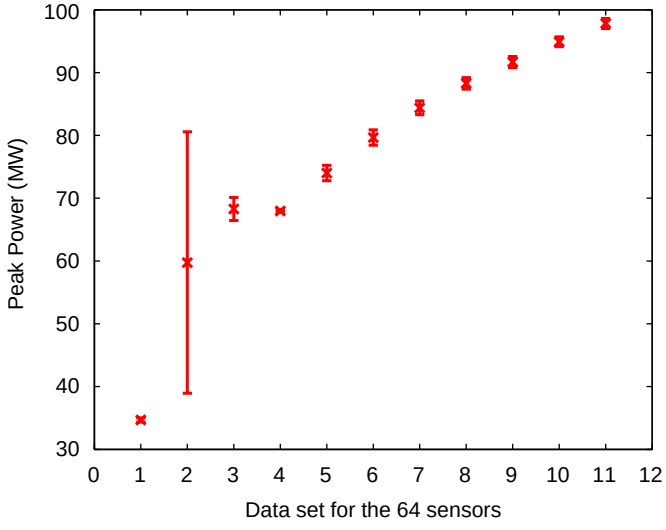

Fig. 11. Standard deviation of the difference between the response in mV of the 64 sensors and their associated fit at a given power and for a given set.

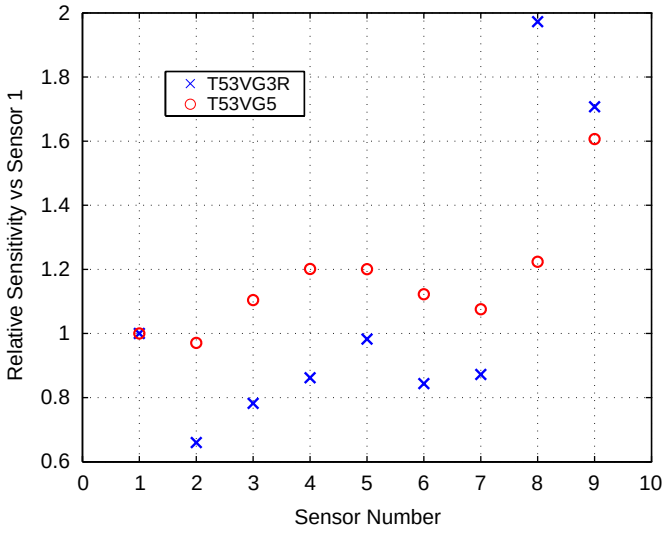

Fig. 12. Sensitivity of the sensors relative to sensor 1 for T53VG3R (crosses) and T53VG5R (circles) structures.

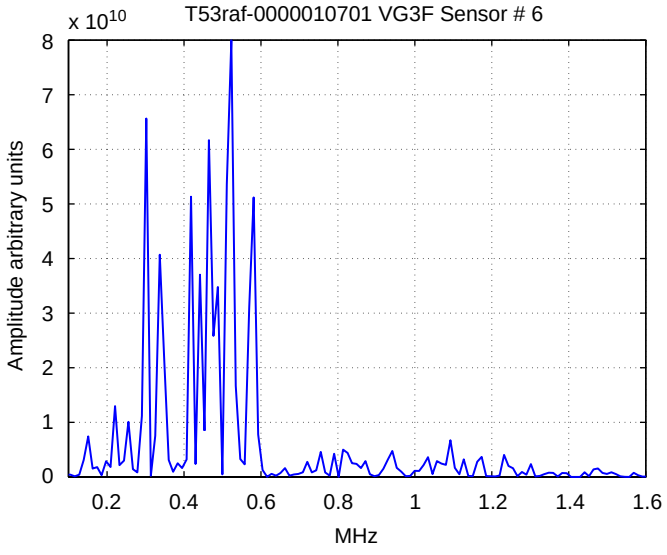

Fig. 13. Fourier transform of the signal of sensor #6 after a recorded breakdown in Fig. 7.

5. Results and discussion

5.1. Limitation of the SLAC-made sensors

In the frequency range of the SLAC-made sensor, Figs. 3 and 4, the wavelength of the phonon lies between 2.4 cm at 200 kHz and 3 mm at 1.5 MHz, assuming a speed for the longitudinal wave of 4760 m/s ($\lambda = c/v$). Fig. 13 shows the frequency response of sensor #6 (Pulse #3) of Fig. 7 on the T53VG3F structure, after a breakdown close to or at, its location. Almost no signal is recorded for frequencies above 1 MHz despite the frequency range of the SLAC sensors (200 kHz to 1.5 MHz). However, those sensors have a higher power attenuation at frequencies above 1.2 MHz cf Fig. 4.

If the sensors are placed too close to each other the frequencies at the low end of the acoustic spectrum will not be resolved. As the radial dimension of the thickness of the iris is comparable to the wavelength of the phonon, diffraction of the wave might occur. The cells have an outside diameter (OD) of ~58 mm and a vacuum beam OD aperture of ~10 mm. The length of a cell is 8.75 mm. The thickness of a cell is ~17.5 mm but the thickness of the iris in the cell is ~1.3 mm, Fig. 2. To avoid diffraction, we can use an acoustic sensor with a higher passband frequency. It has to be mentioned that not all the structures which have been tested have cells of exactly this dimension. However, the values are close.

5.2. Acoustic results

In Fig. 7 a breakdown occurs in pulse #2 ($n-1$) in the middle of the T53VG3F structure, cell 25. The sensors were placed every five cells from the input coupler. This breakdown did not trigger the acquisition and is not included in the total number of breakdowns occurring inside the structure. Also, on the pulse n we can detect two breakdowns. One is happening in the first 10 cells of the structure; the broken sensor 1 cannot permit a more precise determination. The second breakdown is very probably located between cell 25 and 30. The second breakdown, in the same pulse, will not be counted by the RF control software. From this example, we can see how the acoustic emission technique is complementary to the RF analysis of the reflected and transmitted RF power after a breakdown, to locate the cell where the breakdown happened [17].

Due to the quantity of data, automatic analysis is necessary. Simple analysis will calculate the RMS of the first 200 points of the n pulse. The biggest RMS value is then considered to be the location of the breakdown. From this sensor we can compare the other RMS and determine if the second highest RMS value is a valid second breakdown. This automatic method benchmarked with a manual scan of a given sample of data has given very good results. Fig. 14 shows two histograms, one for the T53VG3RA (left) and one for the T53VG3F (right) accelerating structures. Each plot displays the recorded number of breakdowns or events during a given time of RF processing, versus the position in the structure where the event occurred. These results are in good agreement with the RF analysis, Fig. 15. The clusters of dots located on cell 0 and 60 are related to breakdowns attributed to events in the input and output couplers. The dots in between are events localized inside the body of the structure.

This crude analysis gives good coarse results on the localization of the breakdown. Finer results on the localization can be obtain in two ways:

- installing sensors on every cell; and
- extrapolating, and interpolating, the results from the recorded data.

It is easier to install more sensors, however it is expensive in terms of equipment. Refined analysis is therefore a preferable choice. From the raw data, a time analysis can be done. Looking at the bow shape of the signal, Fig. 16, we can estimate the location of the breakdown, if we consider that the acoustic wave is travelling in the copper structure in a straight line at the speed of sound. Data displayed in Fig. 16 were obtained using an earlier acquisition system.

Manual data treatment of the timing information has given very promising results [12]. Automatic treatment of acoustic data in TTF (TESLA Test Facility) in DESY (Germany) [18] has enabled location using few sensors, of the origin of breakdowns, Fig. 17. Due to the complicated geometry of our structures, the automatic timing analysis with the NLCTA data is more challenging. To calculate the time for the breakdown signal to reach the sensor, first the integrated RMS of the first 20 μs of the signal for the breakdown pulse (n pulse), and the RMS for a nominal non-breakdown event (2 pulses before, $(n-2)$) is calculated. Those two values are divided to get a normalized integrated RMS signal. This normalized value is subtracted from the mean of the first microsecond of the breakdown

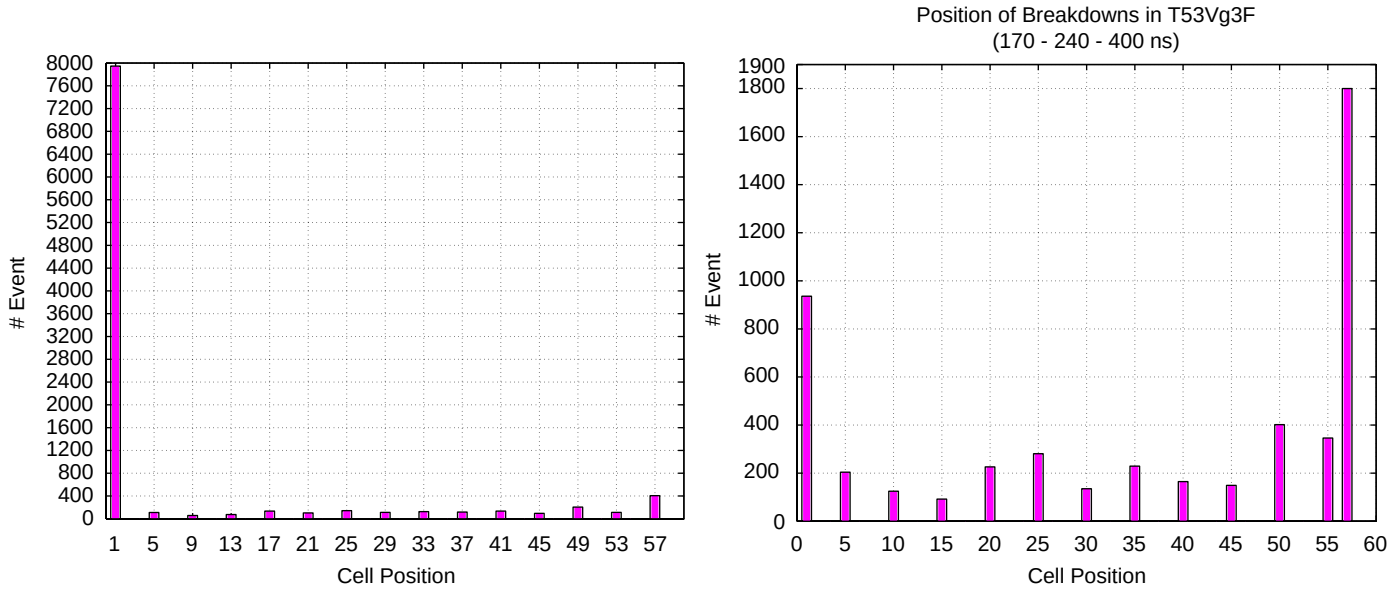

Fig. 14. Number of single breakdown vs location of the 53 cm long RA (left) and F (right) travelling wave structure; for RF pulses of 170, 240 and 400 ns length.

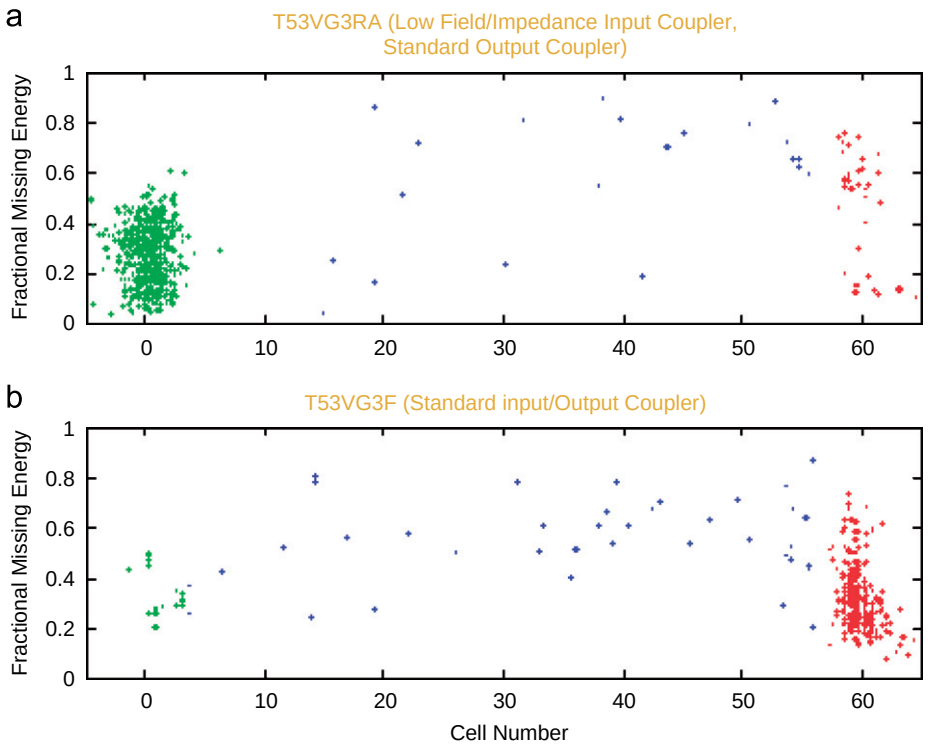

Fig. 15. Localization of RF breakdown by the use of RF analysis. One hundred and twenty hours of operation, at 60 Hz repetition rate, 400 ns pulse width. Electric field: 73 MV/m [17].

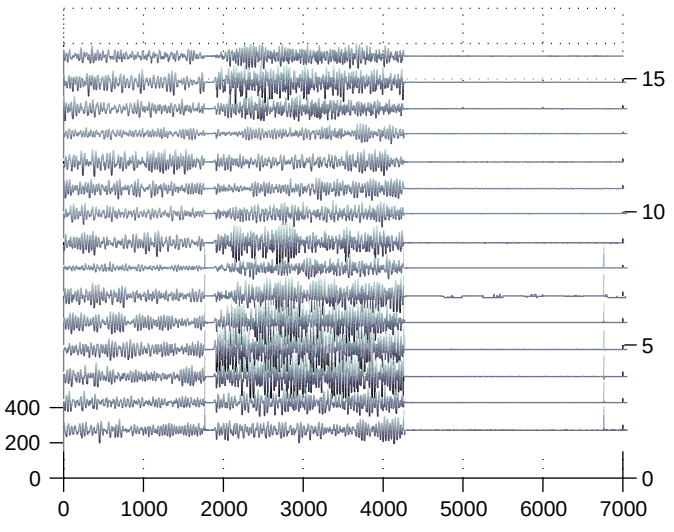

Fig. 16. Multiple RF breakdown in T105VG5, 105 cm long travelling wave structure with 5% group velocity, at 240 ns pulse length. Sensors are located every six cells from cell #2.

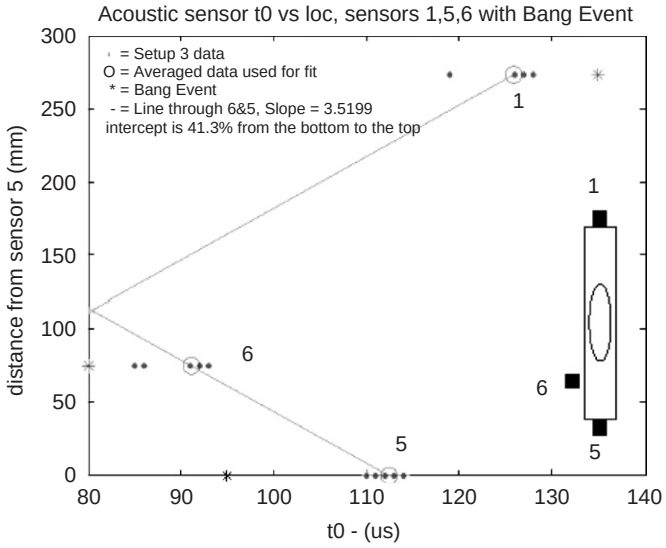

Fig. 17. Sensor distance from sensor 5 vs t0 for the sensors mounted around the periphery of the rectangular waveguide (see lower right hand corner for positioning of the sensors) at its connection point to the coupler cavity. Sixteen events are indicated by the dot symbols and the single large "bang" event is indicated by *. The circles show the mean t0 of the 16 events [18].

pulse signal for every sensor, giving an integrated RMS close to zero. During this first microsecond of the recorded signal, the RF is not yet switched on. The timing is obtained by taking the ratio of the RMS at the n pulse to the RMS of the $(n-2)$ pulse crossing a given threshold.

The gain on the response of the sensor, during a breakdown, has to be well adjusted to avoid saturation of the signal. Not doing so might lead to a wrong calculation of the RMS and inaccurate localization of the breakdown.

The results obtained from the T53VG3RA structure, where more than 75% of the breakdowns are localized in the input coupler, caused us to rearrange the position of our sensors, Fig. 14. It was believed that some breakdowns

were also happening in the arm of the waveguide. As a result a certain number of sensors were moved from the body of the structure to the arms and to the input coupler, Fig. 18. The results of the acquisition are shown in Fig. 19.

A clear asymmetry could be seen each time the input coupler was arcing. This asymmetry was similar to the video data recorded for one of the RF processed Standing Wave (SW) structures [19]. As a result of monitoring activity in structures, we found that most of the breakdowns were localized at the beginning of the structure, Fig. 14 (right) and Fig. 20. The location of single breakdowns in the T105 (travelling wave structure 105 cm long) is presented in Fig. 20. Sensors are located every six cells starting at cell 2. The localization of every breakdown is done manually by analyzing every event and interpolating the timing and the intensity of the response of the sensors. The data shows clearly a serious problem in the input coupler, and also, to a lesser extent in the output coupler.

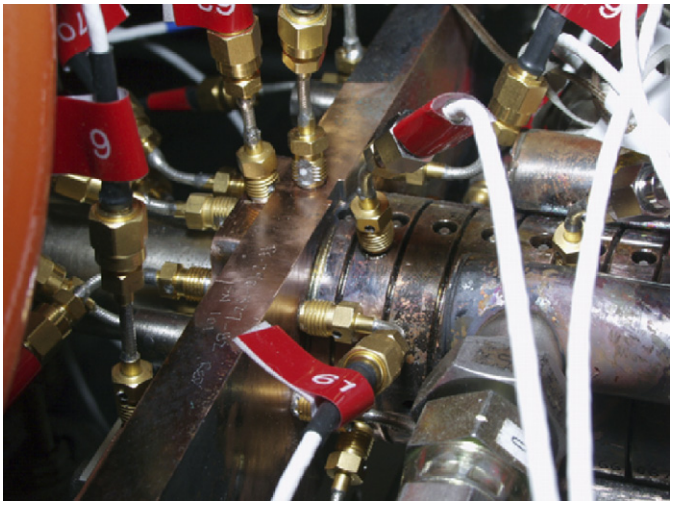

Fig. 18. T53VG3RA structure input coupler closeup.

5.3. *Implication of the acoustic results*

Following the results obtained by the acoustic sensors on the localization of events during RF breakdown as shown for example in Fig. 14, autopsies of the T53VG3R and T53VG3RA structures have been carried out [1]. Extreme damage on the "horns" of the input coupler has been identified, cf Figs. 21 and 22. The horns are the corner separating the waveguide from the cell, as shown in the schematic drawing in Fig. 19. In another travelling wave

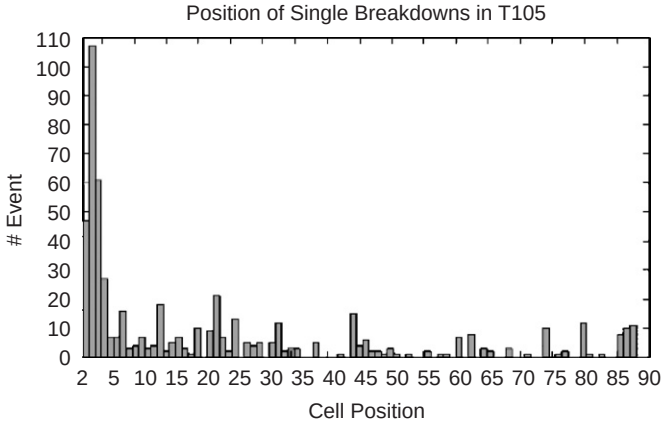

Fig. 20. Manual localization (events vs cell position) of single breakdown inside T105VG5 at 240 ns RF pulse length.

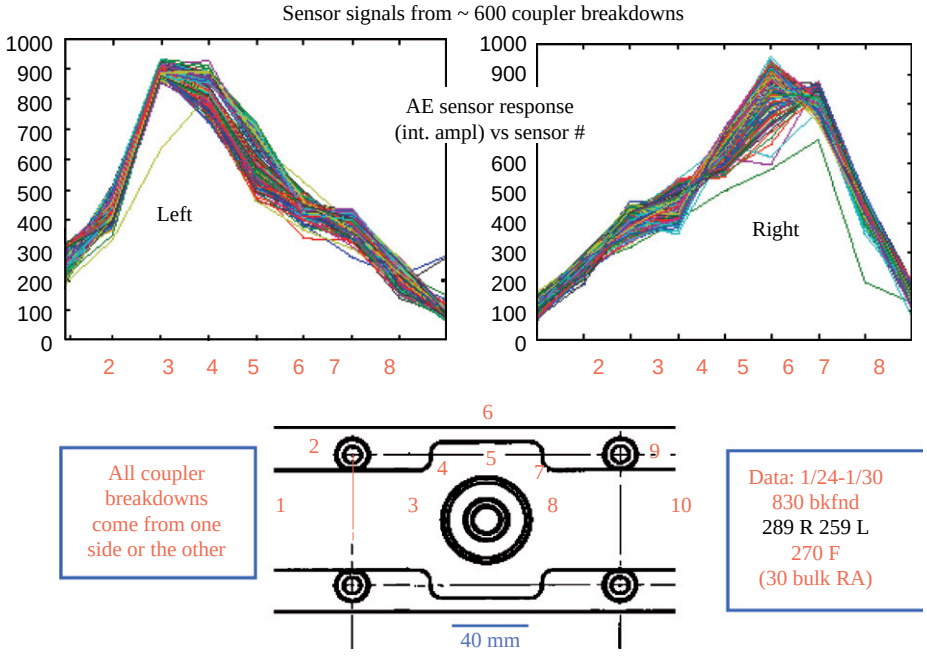

Fig. 19. Localization of breakdown inside the input coupler of T53VG3RA.

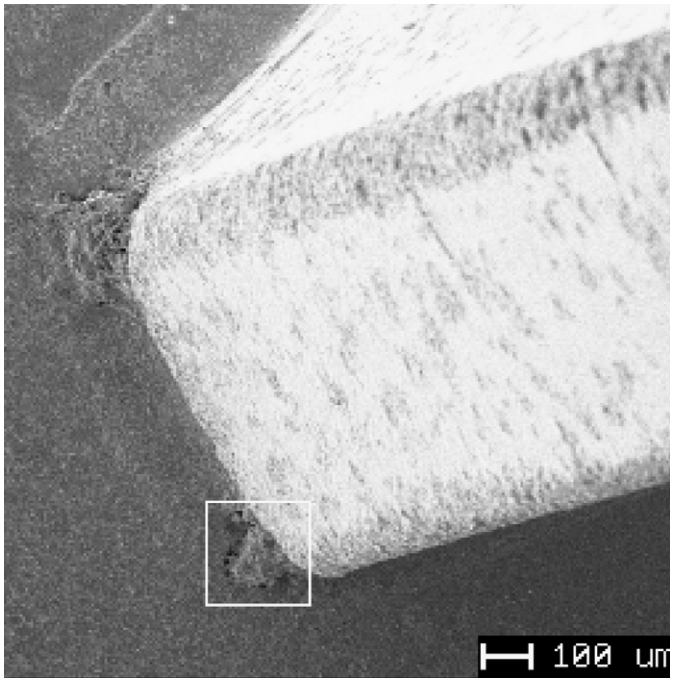

Fig. 21. Autopsy of the upper right horn of the T53VG3RA structure.

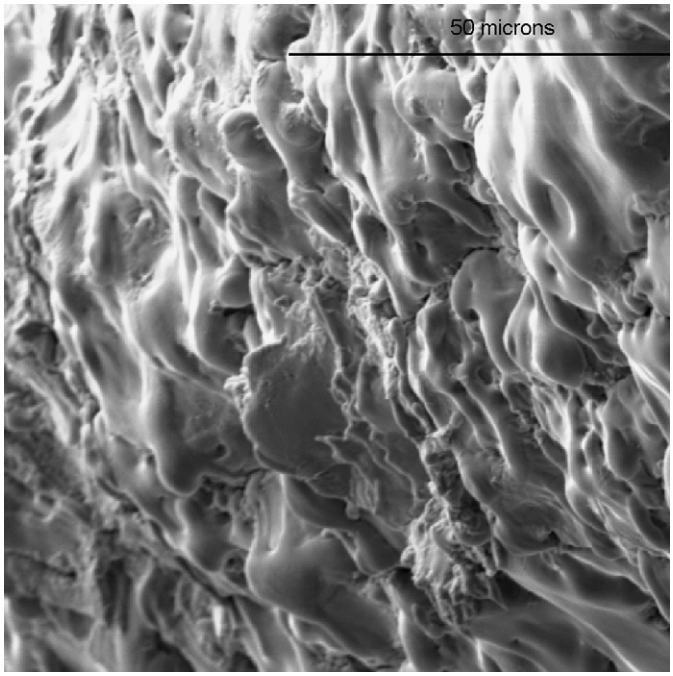

Fig. 22. Typical damage on either edge of the horns, as represented in Fig. 21.

structure (90 cm long 5% group velocity) one cell had more breakdowns than the neighboring cells, cf Fig. 23. As the cross check between RF analysis and the acoustic measurement was not concordant, visual inspection and an autopsy were performed. On the predicted cell, we discovered many craters, indicating more intense activity as well as a piece of aluminium foil sitting on the bottom of

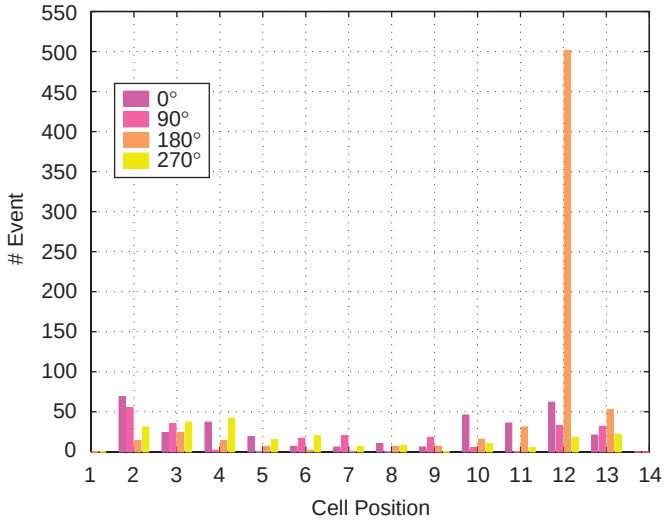

Fig. 23. Position of RF Breakdown in H90VG5 after processing at 50, 100 and 240 ns pulse length. Four acoustic sensors are placed around each cell 90° from each other, and thus on the first 13th cells of the RF structure.

the structure [20], labelled 180° in Fig. 23. Sensors were located in a similar arrangement to Fig. 1, 0° being the top of the structure.

The assistance of the autopsy as a validation of our localization method has led us to better understand the cause of the breakdown occurring inside the input couplers, and especially on the sharp edges of those horns [6]. A new design of the coupler as well as the cells has been implemented for the next structures.

6. Conclusion

Localizing damage by means of ultrasonic measurements is commonly used in the aircraft and building industries. Applying many precisely positioned sensors to localize RF breakdown in accelerator devices is rather new, and we have been able to successfully demonstrate their effectiveness. We have also been able to prove the complementarity of acoustic detection to the conventional RF analysis.

One of the main results has been to identify that breakdowns in the input coupler of our test accelerating structure were happening on the side of the coupler. With the help of surface analysis and some theoretical work [1,6,21] the structure has been redesigned. Localization of pieces of foreign materials inside the structures, has shed light on the handling procedures needed to keep the structures clean. This technique was also used successfully in pinpointing breakdown in the Tesla coupler cavity of the RF photogun.

The next step in using acoustic sensors to understand breakdown, is to develop a good knowledge of the propagation of acoustic waves in annealed copper [22]. This understanding will help with accurate localization, as is possible in superconducting cavities [23]. In other words, this opens up possibilities to study the importance of particulate contamination and surface roughness in

triggering breakdowns. Understanding calibration is understanding the deposition of energy in an event, and being able to account for it. As a result one might have a clearer idea of the relation between damage (phase shift) in the structure and the deposited energy.

Acknowledgments

The authors thank K. Luchini for help on data storage and data preprocessing. K. Ratcliffe's contributions to the NLCTA structure program are also acknowledged. Thanks to E. Kirk(PSI) for proofreading the article. Work was supported by the US Department of Energy under Contract Number DE-AC02-76SF00515.

References

[1] F. Le Pimpec, et al., in: LINAC 2002, Korea, SLAC-PUB-9526, 2002.
[2] M. Gangeluk, et al., Acoustic monitoring system of RF breakdowns inside the electrodynamics structure at Kurchatov SR source accelerator, in: EPAC, P.1986, 1994.
[3] NLC collaboration, Technical Report, SLAC-R-571, 2001.
[4] NLC ZDR Design Group, Technical Report, SLAC Report-474, 1996.
[5] A.D Yeremian, et al., Processing studies of X-band accelerator structures at the NLCTA, in: PAC, Vancouver Canada, 1997.
[6] V. Dolgashev, in: LINAC 2002, Korea, SLAC-PUB-10114, 2002.
[7] D.R. Lide (Ed.), Handbook of Chemistry and Physics, 74th ed., CRC Press, Boca Raton, 1994.
[8] A. Zielinski, Scr. Metall. Mater. 24 (1990) 527.
[9] J.H. Krautkrämer, Ultrasonic Testing of Materials, Springer, Berlin, 1990.
[10] Nondestructive Testing Handbook: Acoustic Emission, vol. 5, second ed., ASNT, 1987.
[11] J. P Wolfe, Imaging Phonons Acoustic Wave Propagation in Solids, Cambridge, 1998.
[12] J. Frisch, et al., in: LINAC 2000, USA, SLAC-PUB-8580, 2000.
[13] J. Frisch, et al., in: LINAC 2002, Korea, SLAC-PUB-9469, 2002.
[14] Standard Method for Primary Calibration of Acoustic Emission Sensors, ASTM International, E1106-86, 2002, pp. 536–547.
[15] P.R. Bevington, D.K. Robinson (Eds.), Data Reduction and Error Analysis for the Physical Sciences, McGraw-Hill, New York, 1992.
[16] J. Tan, Etude de L'émission electronique par effet de Champ en Haute fréquences, Ph.D. Thesis, Université Pierre et Marie Curie Paris 6, 1995.
[17] C. Adolphsen, et al., Results of high power tests 30, in: ISG8, 2002, ⟨http://www-project.slac.stanford.edu/lc/ilc/ISG_Meetings/ISG8/wg4.htm⟩.
[18] J. Nelson, M. Ross, Technical Report, SLAC-PUB-9340, 2001.
[19] M. Ross, et al., Measurement of RF breakdown in X-band structures, in: LC02 Workshop SLAC, 2002, ⟨http://www-conf.slac.stanford.edu/lc02/wg2/WG2_Ross.pdf⟩.
[20] S. Harvey, et al., J. Vac. Sci. Technol. A22 (4) (2004).
[21] D. Pritzkau, RF pulsed heating, Ph.D. Thesis, Stanford University, SLAC-report-577, 2001.
[22] G. Gollin, Acoustic techniques for studying high-voltage breakdown, ⟨http://web.hep.uiuc.edu/home/g-gollin/research/acoustic.html⟩.
[23] J. Knobloch, Advanced thermometry studies of superconducting RF cavities, Ph.D. Thesis, Cornell University, 1997.